Effective model for the electronic properties of quasi-one-dimensional purple bronze $Li_{0.9}Mo_6O_{17}$ based on *ab initio* calculations

Martin Nuss* and Markus Aichhorn

Institute of Theoretical and Computational Physics, Graz University of Technology, 8010 Graz, Austria

(Received 10 June 2013; revised manuscript received 18 December 2013; published 16 January 2014)

We investigate the electronic structure of the strongly anisotropic, quasi-low-dimensional purple bronze $Li_{0.9}Mo_6O_{17}$. Building on all-electron *ab initio* band-structure calculations, we obtain an effective model in terms of four maximally localized Wannier orbitals, which turn out to be far from atomiclike. We find *two half-filled* orbitals arranged in chains running along one crystallographic direction and *two full* orbitals in perpendicular directions, respectively. The possibility to reduce this model to only two orbitals forming two chains per unit cell with interchain coupling is discussed. Transport properties of these models show high anisotropy, reproducing trends of the experimentally determined values for the dc conductivity. We also consider basic effects of electron-electron interactions using the (extended) variational cluster approach and dynamical mean field theory. We find good agreement with experimental photoemission data upon adding moderate onsite interaction of the order of the bandwidth to the *ab initio* derived tight-binding Hamiltonian. The obtained models provide a profound basis for further investigations on low-energy Luttinger-liquid properties or to study electronic correlations within computational many-body theory.

DOI: 10.1103/PhysRevB.89.045125 PACS number(s): 71.10.−w, 71.27.+a, 71.20.−b, 72.15.−v

I. INTRODUCTION

The electronic structure of highly anisotropic materials shows a plethora of interesting effects. Quantum many-body dynamics in quasi-low-dimensional systems becomes important and dominant in many regions of their rich phase diagram. This often implies unconventional ground states, such as non-Fermi-liquid or Luttinger-liquid states. One prominent example for this class of materials is the lithium molybdenum purple bronze $Li_{0.9}Mo_6O_{17}$ [1], a molybdenum oxide bronze with quasi-one-dimensional properties. [2]

Experimental structure analysis using x rays [3] as well as neutrons [4] determined a monoclinic crystal structure. The conduction electrons are mostly located on two molybdenum octahedral sites which are arranged in double zigzag chains along the *b* axis. This leads to a very high anisotropy of the material, which has been studied by several techniques using resistivity measurements [5–10], conductivity under pressure [11], magnetoresistance [8,12], thermal expansion [13], optical conductivity [14,15], the Nernst effect [16], thermal conductivity [17], thermopower [18], and muon spectroscopy [19].

The electronic properties have been addressed using angle-resolved photoemission spectroscopy (ARPES) [20–28] and scanning tunneling microscopy (STM) [29,30], which argued for one-dimensional Luttinger-liquid physics [28,31–36]. Other studies disputed this claim [37]. The evolution and the current status of work in that direction is summed up in a recent review article [26]. A temperature-dependent dimensional crossover [38–40], which induces coherence for the perpendicular electron motion, has been studied using neutron diffraction [4].

Apart from intriguing physical effects of effective low dimensionality, the material shows superconductivity below 1.9 K [2,41–44] and a metal-insulator transition is observed at around 24 K [5,14,41,45]. No evidence for a Peierls instability has been reported [46], and a possible charge-density wave (CDW) phase is still under debate [29,47–49]. Recent studies have argued for a compensated metal [50]. All data are summed up in a conjectured electronic phase diagram as presented in [49].

Theoretical *ab initio* studies of the electronic structure using a tight-binding method [51] as well as a linearized muffin-tin orbital (LMTO) [52,53] calculation in the local density approximation (LDA) have been conducted. These approaches were successful in providing a broad picture of the "high-energy" physics of $Li_{0.9}Mo_6O_{17}$, accounting for the high anisotropy. Although experiments testified a wealth of remarkable low-energy properties and different quantum ground states, more detailed theoretical investigations, including interactions and low dimensionality, emerged in recent years only.

Chudzinski *et al.* [48] investigated the quasi-one-dimensionality and have been able to extract an effective *low-energy* theory within the Tomonaga–Luttinger-liquid framework. Their approach is based on an atomic orbital tight-binding model with parameters such that it matches an LDA LMTO band-structure calculation. Motivated by the crystal structure of $Li_{0.9}Mo_6O_{17}$, the model was set up with four molybdenum *d* orbitals in a zigzag ladder arrangement including onsite as well as nonlocal electronic interactions. It was found that within this model, Luttinger-liquid low-energy parameters can be obtained, which are consistent with experimental findings.

Another recent work [49] proposes a two-dimensional model from *Slater-Koster* [54] atomic orbitals also including nonlocal electronic interactions. Again, an ansatz with four Mo orbitals in zigzag ladder arrangement was applied. The authors argue, based on electron counting, that there are two electrons to be shared among the four equivalent Mo atoms, leading to quarter-filled orbitals. The bandwidth obtained with this ansatz for the two bands crossing the Fermi level is in rough agreement with density functional theory (DFT) calculations.

*martin.nuss@student.tugraz.at

Details of the band structure such as curvatures, however, and also the bands just below the Fermi level which are of similar Mo d character, can not be reproduced by this *Slater-Koster* model.

The main purpose of this work is to establish an unbiased, *general purpose tight-binding model* for the electronic properties of $Li_{0.9}Mo_6O_{17}$ based on *ab initio* calculations. Such a model is intended to serve as a basis to study the role of electronic correlations by adding interactions, be it in a computational many-body theory or in a one-dimensional renormalization group (RG) framework. In contrast to previous work [49], we propose a model based on maximally localized Wannier orbitals [55,56] instead of linear combination of atomic orbitals. Four molecularlike orbitals are obtained in a fully *ab initio* approach from an all-electron DFT calculation. Our results unambiguously show that, using a set of four Wannier orbitals in the unit cell, the model consists of *two half-filled* as well as *two filled* orbitals. As we will show in the following, the DFT band structure is perfectly reproduced in this basis set of Wannier functions.

This model describes the momentum-resolved electronic structure as observed in ARPES [22] experiments and reproduces highly anisotropic transport characteristics [5–8,12,14,17]. Furthermore, we discuss an even simpler two-orbital effective model which can be derived from the four-orbital model.

In the second part of the paper, we conduct a first (qualitative) study of effects of interactions on the electron dynamics within this effective Wannier model. Even more so due to the low dimensionality, the interacting model is in general difficult to approach. By applying RG as well as density matrix renormalization group (DMRG) [57] in certain limits (chains, ladders), their essential physics can be understood [49]. To solve the full low-dimensional interacting Hubbard-type model, general frameworks as for example (cluster) dynamical mean field theory [(C)DMFT]-like approaches [58] have been applied, where the self-energy of the system is restricted to a finite length scale.

Realistic modeling is a relatively new and rapidly developing field [60–62]. In this work, we study (simple) electron-electron interactions in the effective model using complementary numerical techniques. First, we use cluster perturbation theory (CPT) [63,64] as well as the (extended) [65,66] variational cluster approach [67] [(e)VCA] in the spirit of LDA + VCA [68,69]. The choice of these methods is motivated by the expected reduced effective dimensionality of the material which renders the nonlocal character of the VCA self-energy an interesting perspective. Second, we apply the well-established LDA + DMFT [70–72] approach, which neglects nonlocal correlations, but on the other hand performs superior in describing the quasiparticle features at low energy as compared to VCA. For all applied methods, we find that a moderate value of onsite interactions strength is capable of describing the electron dynamics best and in good agreement with ARPES experiments. We discuss the influence of a hybridization mechanism of the two bands right at the Fermi energy with the two bands slightly below, not accounted for in previous work.

This paper is organized as follows: In Sec. II, we report accurate all-electron DFT data from which we obtain a model in terms of maximally localized Wannier functions. A further simplified model for $Li_{0.9}Mo_6O_{17}$ with reduced number of hopping parameters is discussed in Sec. II C. We present results for the anisotropic conductivity in Sec. III and compare to transport measurements. The electron dynamics of the interacting effective model is presented and compared to ARPES experiments in Sec. IV before concluding in Sec. V.

II. FROM CRYSTAL STRUCTURE TO AN EFFECTIVE ELECTRONIC MODEL

A. *Ab initio* electronic structure

We obtain the electronic structure for ideal $Li_1Mo_6O_{17}$ from a non-spin-polarized, full-potential linearized augmented plane wave (FP-LAPW) [73–76] DFT [77,78] calculation as implemented in the WIEN2K package [79]. The unit-cell parameters and crystal structure are taken from x-ray data [3] which have been recently confirmed by neutron diffraction experiments [4]. The space group is monoclinic (prismatic) $P2_1/m$ with lattice parameters $a = 12.762(2)$ Å, $b = 5.523(1)$ Å, $c = 9.499(1)$ Å, $\beta = 90.61(1)^\circ$, and $Z = 2$, leading to a 48-atom unit cell $[Li_1Mo_6O_{17}]_2$ [80].

All results presented in this work are calculated with the exchange-correlation potential treated in the LDA [81]. We checked that the generalized-gradient approximation (GGA-PBE [82]) gives indistinguishable results for the band structures. Our results are converged in terms of the size of the FP-LAPW basis set, which is determined by the $RK_{\max}$ parameter in WIEN2K. By performing calculations for different $RK_{\max}$ we found that $RK_{\max} = 7.0$ and 6.0 gave the same results, with band energies within 10^{-3} eV, only at $RK_{\max} = 5.0$ deviations become visible. Therefore, also due to the computational complexity of the problem, all results presented here are obtained with a $RK_{\max} = 6.0$ basis set.

The obtained electronic structure $\epsilon_{\mathrm{KS}}(\mathbf{k})$ is visualized along the standard path of the b-c plane in reciprocal space (Y-G-X-M) (see also Fig. 2) in Fig. 1 (left). In order to compare to ARPES experiment, we modeled lithium-vacant $Li_{0.9}Mo_6O_{17}$ by a rigid band shift of 0.03 eV of the LDA bands [52]. We find a combined bandwidth of the four bands in the vicinity of the Fermi energy ϵ_F of $W \approx 1.82$ eV and two Fermi velocities of $v_{F,1} \approx 0.99 \times 10^5$ m/s and $v_{F,2} \approx 0.93 \times 10^5$ m/s, roughly one order of magnitude lower than in free-electron metals [83]. The corresponding electronic density of states (DOS) is shown in Fig. 1 (right). The LDA DOS is obtained by Gaussian integration ($\sigma \approx 0.02$ eV) using the tetrahedron method on a grid of 216 k points in the irreducible Brillouin zone (BZ).

By and large, the electronic structure compares well to previous data reported in early works of Whangbo *et al.* [51] from an empirical tight-binding method, and also to more recent LMTO calculations within the atomic sphere approximation (ASA) from Popovic *et al.* [52]. But note that in particular the band crossings/hybridizations on the X-M line as well as the lowest empty bands at $\sim$1 eV above ϵ_F are apparently different. Since we checked accurately the convergence of the all-electron FP-LAPW calculations, the difference is most likely to come from the approximations introduced in LMTO-ASA and tight-binding calculations.

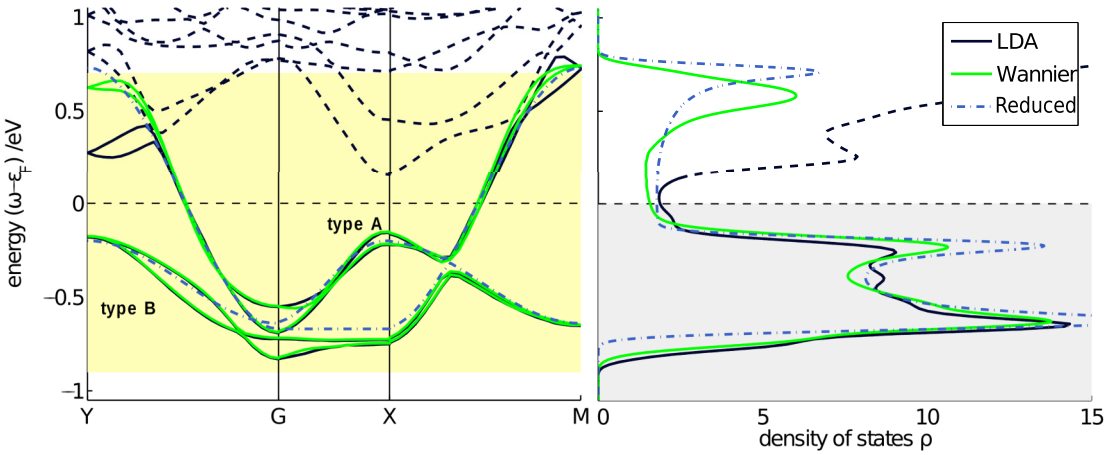

FIG. 1. (Color online) Left: LDA band structure (solid black) in the vicinity of the Fermi energy ϵ_F plotted along a two-dimensional path in the reciprocal b-c plane. The four bands of the full Wannier projected Hamiltonian are shown on top (solid green) next to the data for the reduced model (dashed-dotted blue line). Right: DOS of the LDA calculation (black), the full Wannier model (solid green line), and the reduced model (dashed-dotted blue line).

The one dimensionality of the material becomes manifest in the Fermi surface which is shown in Fig. 2 (left). Arising from two bands crossing the Fermi energy, it consists of two sheets warping in the c direction, cutting the b axis and being roughly constant in the a direction. In experiments [84], the maximum splitting of the Fermi surface ($<10^{-3}$ Å^{-1}) is observed along the $\overline{\text{PK}}$ line. Our LDA calculations yield the maximum splitting along the very same line (see Fig. 2), but the magnitude is much larger ($\approx$0.021 Å^{-1}). In previous LDA calculations [52], an even larger splitting of $\approx$0.045 Å^{-1} was found. This discrepancy of the theoretical results with experiment is likely due to the improper treatment of strong nonlocal electronic correlations in the LDA.

B. Realistic effective model

To construct an effective model, we have to identify the origin (orbital character and atom) of those electronic states which are most important for the physical properties, i.e., those close to the Fermi energy ϵ_F. We plot in the bottom panel of Fig. 3 the partial DOS for the six inequivalent Mo atoms in the unit cell. One can nicely see that Mo_1 and Mo_4 contribute most to the DOS at ϵ_F (for nomenclature see Fig. 2 in Onoda *et al.* [3]). In the top panel of Fig. 3, we show the crystal structure, with emphasis on those Mo_1 and Mo_4 (including the equivalent Mo_1' and Mo_4') atoms. It is evident that these atoms form the two adjacent zigzag chains running along the b axis, giving rise to the two quasi-one-dimensional bands crossing ϵ_F. The atoms Mo_2 and Mo_5 are sitting next to the chains, and thus have some smaller contributions. The other two Mo atoms are far away from the chains, and thus contribute hardly anything to the weight around ϵ_F. This analysis of the orbital character shows clearly that the bands around ϵ_F originate mainly from only four atoms (Mo_1, Mo_4 and Mo_1', Mo_4', respectively) in the unit cell.

To construct an effective model, we take the electronic wave-function data $\boldsymbol{\phi}_{\text{KS}}$ in an energy window of $[-0.9, 0.7]$ eV, that comprises the four relevant bands as shown in Fig. 1. The lower bound of the energy window for projection is straightforward to choose because the gap between the four

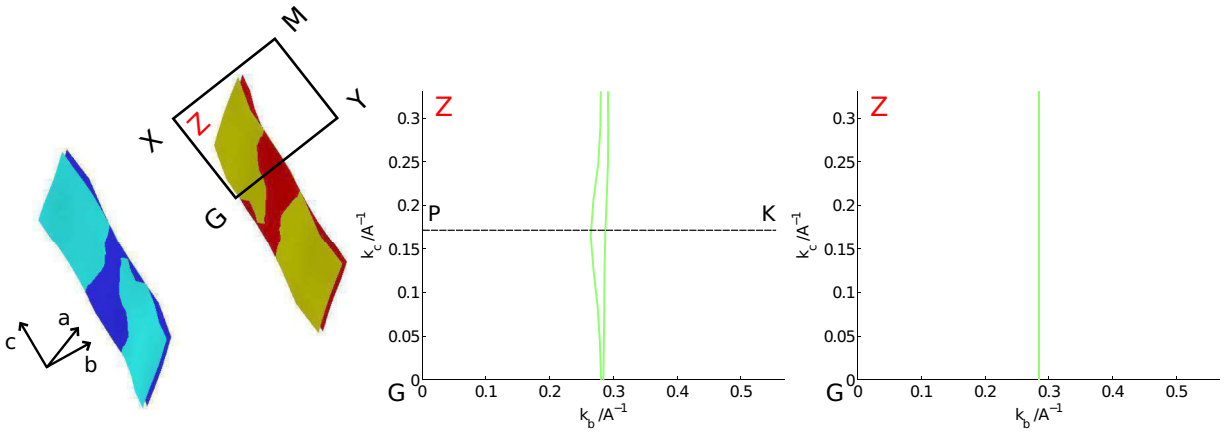

FIG. 2. (Color online) Calculated Fermi surface. Left: The *ab initio* result (image created using XCRYSDEN [59]). Center: In-plane projection of the result for the four-orbital Wannier model. Right: In-plane projection of the result for the reduced model, where type-A orbitals are strictly one dimensional and the two Fermi sheets are degenerate.

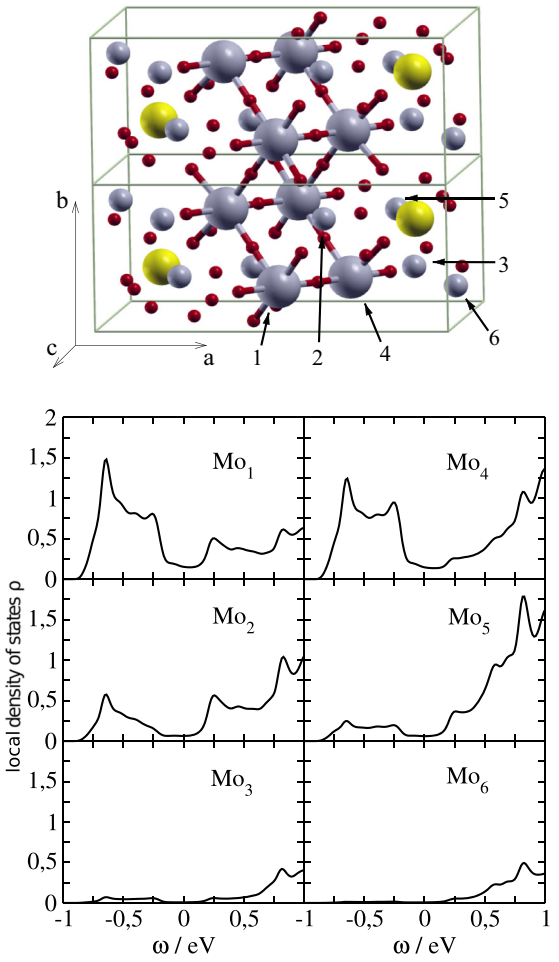

FIG. 3. (Color online) Top plot: Crystal structure. In the a and c directions one unit cell and in the b direction two unit cells are shown. Big gray balls are Mo_1/Mo_1' and Mo_4/Mo_4' atoms, showing the zigzag chain structure along b. Small gray: other Mo sites. The numbers next to the black arrows denote the atom number. Small red balls are oxygen, and the yellow balls Li atoms. This image has been created using XCRYSDEN [59]. Bottom plot: Partial DOS of the six inequivalent Mo atoms in the unit cell. Top row: atoms Mo_1 and Mo_4, forming the zigzag chains. Middle row: Mo_2 and Mo_5. Bottom row: Mo_3 and Mo_6.

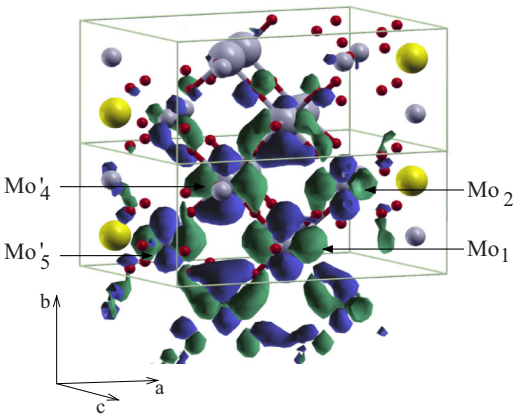

FIG. 4. (Color online) Visualization of one type-A Wannier orbital. Similar as in Fig. 3, two unit cells in the b direction are shown, the Wannier function is centered in the lower unit cell. The center of the Wannier function is located in-between atoms Mo_1 and Mo_4'. Arrows mark the atoms with significant contribution to the Wannier function: in-chain atoms Mo_1 and Mo_4', and adjacent atoms Mo_2 and Mo_5'. Color coding as in the top panel of Fig. 3. For the Wannier functions, blue and green lobes denote positive and negative phases, respectively. The image has been created using XCRYSDEN [59].

considered molybdenum d bands and the next lower bands is larger than 1.5 eV. The upper bound is more involved since bands with different character penetrate the energy window from above, and are entangled with the two bands crossing the Fermi energy. In order to get a good description of the bands, we had to use the disentanglement procedure of WANNIER90 with a frozen energy window of $[-0.9,0.0]$ eV.

We project these data onto four maximally localized Wannier orbitals [55] ω_α using WANNIER90 [85] and the WIEN2WANNIER [86] interfaces. As initial seed, we chose one d_{xy} orbital on each of the Mo_1, Mo_4, Mo_1', and Mo_4' atoms.

Although starting from a seed with atomic orbitals, the calculated Wannier functions, however, have quite different character. They can be divided into two kinds. Type A, which is oriented along chains in the b direction, and type B which is in some sense orthogonal in real space, mediating between the chains in the b direction. The orbitals contributing to the states around ϵ_F are of type A, and one of these orbitals is shown in Fig. 4. One can clearly see the d_{xy} orbital character, forming the zigzag chains, around atoms Mo_1 and Mo_4', where most of the orbital weight is located. In consistency with the partial DOS (Fig. 3), some contribution also comes from atoms Mo_2 and Mo_5' since they are adjacent to the chains, as shown in Fig. 4.

The splitting into two types of orbitals can be understood from the band structure. Only two bands cross ϵ_F, which results in two equivalent Wannier functions (A). The other two bands, lying below ϵ_F, are spanned by another set of two equivalent Wannier functions (B), respecting the crystal symmetry.

We would like to emphasize that these orbitals are far from atomiclike. We estimate their spread from the square root of the spread functional of WANNIER90, which yields 5.2 Å for orbital type A, and 4.4 Å for orbital type B. We also want to note that the Wannier functions are not centered on a Mo site. Instead, Fig. 4 clearly shows that the centers are located in the middle of a bond between two Mo sites. For type A, one orbital has its center between atoms Mo_1 and Mo_4', the other between Mo_1' and Mo_4, respectively. In that sense, these Wannier orbitals can be regarded as bond-centered molecularlike orbitals.

The origin of the large spread in real space is the very limited number of bands that are taken into account in the Wannier construction scheme. Taking all d orbitals of the Mo_1, Mo_1', Mo_4, and Mo_4' atoms as well as the bridging oxygen p orbitals into account would of course result in much better localization. However, the Hamiltonian then describes many bands, and not only the most important four bands in the vicinity of ϵ_F. A similar effect can be observed for instance in the construction of the one-band model in cuprate superconductors. Also there, taking only the $d_{x^2-y^2}$ orbital into the construction results in quite large Wannier orbitals with long tails [87].

Concerning the electron charge in the Wannier orbitals, we find that orbitals of type A are *half-filled*, whereas orbitals of type B are identified as (almost) filled. For lithium-vacant purple bronze, we find a total occupation of ≈5.8 electrons in these four bands since there are two lithium ions in the unit cell, each contributing ≈0.1 hole doping. In the remainder of the paper, we will therefore use for all discussions an average filling of the four bands of $\langle n \rangle = 1.44$ [88].

Specifically, the downfolding procedure yields the matrix elements of a single-particle Hamiltonian [89]

$$H_{\mathrm{Wannier},\alpha\beta}(\mathbf{k}) = \langle \omega_\alpha | \, \hat{\mathcal{H}}_{\mathrm{Wannier}}(\mathbf{k}) \, | \omega_\beta \rangle = \sum_{\delta R} e^{-i\mathbf{k}\cdot\delta R} M_{\mathbf{R}\alpha\mathbf{R}'\beta} \quad (1)$$

in the four-orbital Wannier space $\alpha,\beta = \{\mathrm{A},\mathrm{A}',\mathrm{B},\mathrm{B}'\}$ where the sum runs over all lattice translations $\delta R = (\mathbf{R} - \mathbf{R}')$ and the crystal momentum $\mathbf{k}$ is defined in the first BZ [90].

Our model (1) consists of two filled electronic orbitals, type B, slightly below the Fermi energy ϵ_F ($M_{\mathbf{0B0B}} = M_{\mathbf{0B'0B'}} = -0.423$ eV), as well as two half-filled ones, type A, crossing the Fermi energy ϵ_F ($M_{\mathbf{0A0A}} = M_{\mathbf{0A'0A'}} = 0.005$ eV). The largest energy scale for the hopping matrix elements is the nearest-neighbor hopping along the b direction of orbitals of type A which is $t_{\max} \approx -0.35$ eV.

This 4×4 noninteracting Wannier Hamiltonian can easily be diagonalized by numerical means. Its band structure and DOS are plotted on top of the LDA results in Fig. 1. The Wannier DOS has been calculated from $N_{1.\mathrm{BZ}} = 48^3$ k points in the first BZ, using a numerical broadening of $0^+ = 0.086\, t_{\max}$. We obtain very good agreement except for the upper band edges, where the accuracy is influenced by the entanglement of the bands in this energy region. We find a total bandwidth of the four bands in the vicinity of ϵ_F of $W \approx 1.57$ eV and two Fermi velocities of $v_{F,1} \approx 1.16 \times 10^5$ m/s and $v_{F,2} \approx 1.06 \times 10^5$ m/s. Note that the Fermi velocity is pointing along the b direction, while the other components are three orders of magnitude smaller. The Fermi surface (see Fig. 2, center) is also reproduced very accurately by the Wannier model.

C. Effective interchain coupling

The Wannier model (1) consists of numerous single-particle hopping terms between four Wannier orbitals in a three-dimensional crystal. Many of the terms of the Wannier model are orders of magnitude smaller than the dominant hopping process of type-A orbitals along the b direction with $t_{\mathrm{AA}} \approx -0.35$ eV. For instance, all intra-unit-cell hybridizations are negligibly small (of order 10^{-4} eV). This includes direct hopping $t_{\mathrm{AA}'}$ between adjacent chains. The reason for this is that the two orbitals type A and A′ are aligned parallel to each other in the unit cell, with negligible overlap. The hybridization perpendicular to the chains, which is responsible for the dispersion in perpendicular direction, is predominantly mediated through the type-B orbitals in an (A-B-A) or (A-B-A′) fashion (see Fig. 5). In this section, we derive a two-dimensional model in the b-c plane consisting of two degenerate half-filled chains that comprises the fundamental

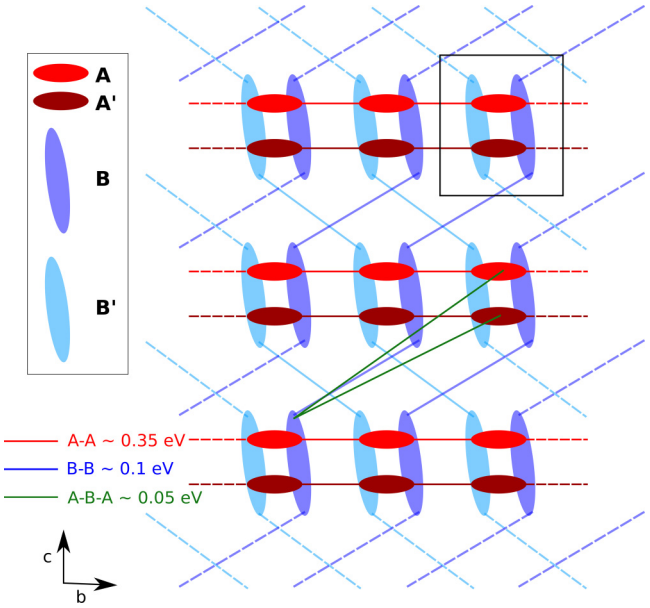

FIG. 5. (Color online) Visualization of the full effective Wannier Hamiltonian (1). A schematic drawing of the most dominant hopping processes is presented: type-A orbitals (red), type-B orbitals (blue). Lines denote the dominant hopping paths, and the black square marks the size of the unit cell.

model. The indirect hopping results only in a small effective hopping between the chains, which we estimate perturbatively.

The starting point for perturbation theory is a Hamiltonian, where orbitals of type A and type B are decoupled. For this purpose we define a complete set of projection operators projected Hamiltonians $\hat{\mathcal{H}}_{\alpha\alpha} = \hat{P}_\alpha \hat{\mathcal{H}} \hat{P}_\alpha$ on the type $\alpha = \{\mathrm{A},\mathrm{B}\}$ orbitals. In zeroth-order approximation, the hybridization terms are set to zero, $\hat{\mathcal{H}}_{\mathrm{AB}} = \hat{\mathcal{H}}_{\mathrm{BA}} = 0$. For our Wannier model, this corresponds to neglecting those matrix elements which are less than 10% of the largest occurring hopping energy $|t_{\max}| = 0.35$ eV and leads to a Hamiltonian

$$H_{\mathrm{reduced}} = \begin{pmatrix} t_{\mathrm{AA}} 2\cos(k_b b) & 0 \\ 0 & \epsilon_B + t_{\mathrm{BB}} 2\cos(k_b b \pm k_c c) \end{pmatrix}, \quad (2)$$

with $t_{\mathrm{AA}} = -0.35$ eV, $t_{\mathrm{BB}} = -0.11$ eV, and $\epsilon_{\mathrm{B}} = -0.45$ eV accompanied by the rigid band shift of $\mu = -0.03$ eV. One has to keep in mind that both bands A and B are doubly degenerate. We will refer to this Hamiltonian as *reduced model* throughout this work.

Note that the two type-B orbitals disperse in orthogonal diagonals. The bands crossing the Fermi energy arise due to the two degenerate type-A orbitals which now represent isolated, one-dimensional chains dispersing in the b direction. Due to the missing hybridization between A and B orbitals, fine features of the perpendicular (c-direction) dispersion are not reproduced. Nevertheless, despite its simplicity, the band structure and density of states (see Fig. 1) are still described very well. Data in the figure have been obtained using $N_{1.\mathrm{BZ}} = 48^3 k$ points in the first BZ and a numerical broadening of $0^+ = 0.086\, t_{\max}$ for the evaluation of the DOS.

We find a bandwidth of the two bands in the vicinity of ϵ_F of $W \approx 1.4$ eV and a Fermi velocity of $v_F \approx 0.93 \times 10^5$ m/s.

In order to estimate the effective interchain coupling, we treat the indirect (A-B-A′) hoppings in second-order perturbation theory. For that purpose, we project the full four-orbital Wannier model (1) onto the type-A bands [91]

$$\hat{\tilde{\mathcal{H}}}_{\mathrm{AA}} = \hat{\mathcal{H}}_{\mathrm{AA}} + \hat{\mathcal{H}}_{\mathrm{AB}}(\omega - \hat{\mathcal{H}}_{\mathrm{BB}})^{-1}\hat{\mathcal{H}}_{\mathrm{BA}}\,.$$

Upon approximating ω by the bare eigenenergies of $\hat{\mathcal{H}}_{\mathrm{AA}}$, we arrive at a two-orbital model which reproduces the band dispersions of the two bands crossing the Fermi energy (not shown). We note in passing that this two-orbital model can also be obtained by a Wannier construction where the basis is restricting to bands of type A alone.

Keeping the number of hopping terms low, we now perform a fit of $\hat{\tilde{\mathcal{H}}}_{\mathrm{AA}}(\mathbf{k})$ with a Hamiltonian that contains perpendicular hopping in addition to the terms of the A orbitals of the reduced model [Eq. (2)] respecting the symmetry of the lattice. In particular, we choose for the perpendicular hopping both intrachain (A-A) terms as well as interchain (A-A′) terms. The χ^2 fit is done using 20^2 k points on an equidistant grid in one fourth of the reciprocal b-c plane ($k_a \approx 0$) plus 3×32 k points on the standard path Y-G-X-M. The only relevant perpendicular hopping processes given by this procedure are nearest-neighbor interchain terms of the order of $t_{\mathrm{AA}'} \approx -0.005$ eV, as well as nearest-neighbor intrachain terms of the order of $t_{\mathrm{AA}} \approx -0.02$ eV. The hopping in the b direction only slightly renormalizes to $t_{\mathrm{AA/A'A'}} \approx -0.37$ eV accompanied by an onsite shift of $\epsilon_{\mathrm{A/A}'} = -0.01$ eV.

Thus, we find an intuitive two-orbital model that consists of two chains dispersing in the b direction with nearest-neighbor perpendicular hoppings of type A-A and A′-A′ which are one order of magnitude smaller than the hopping in the b direction. The direct effective hopping of type A-A′ between the two chains within one unit cell is again one order of magnitude smaller. This small effective coupling explains the robust one dimensionality of the compound. Our calculated values are in good agreement with those discussed in [48].

We want to stress here that only in this section fitting of parameters was performed, in order to estimate the effective perpendicular hopping using only a few parameters. In all other parts of this work, only *ab initio* calculated hopping integrals are used.

III. ANISOTROPIC CONDUCTIVITY

We augment our discussion of the electronic structure by computing the linear response transport and comparing it to experiments. The conductivity tensor of $Li_{0.9}Mo_6O_{17}$ consists of three independent diagonal σ_a,σ_b,σ_c entries as well as one nonzero off-diagonal element $\sigma_{bc} = \sigma_{cb}$ (see Appendix A). Literature provides values for the anisotropic resistivity at room temperature (300 K) and zero magnetic field using several experimental techniques. We summarized the reported data in Table I which all agree on a highly anisotropic resistivity. The ratio between the diagonal elements of the resistivity tensor, however, strongly disagrees in-between the individual measurements. In particular, $\rho_a : \rho_b$ differs by a factor of ≈60 while $\rho_b : \rho_c$ differs even by a factor of ≈640 from the lowest to the highest anisotropy found in experiments. These discrepancies are often attributed to experimental challenges when measuring the resistivity of strongly anisotropic small samples.

TABLE I. Collected data for the anisotropic resistivity at $T = 300$ K and our low-temperature theoretical results for small scattering γ[eV] ∼ 0.05 eV. Data from Refs. [5,12,14] were obtained via four-point measurements, Refs. [6,7] report results using the Montgomery method, Ref. [8] measurements are based on magnetoresistance, and in Ref. [17] a Hall experiment was carried out. Resistivity values which were not given in the respective publications are represented by dashes in the ratio column.

Ref.	ρ_a m Ωcm	ρ_b m Ωcm	ρ_c m Ωcm	Ratio
[5]	2470	9.5		260:1:-
[12]	64.5	16	854	4.5:1:50
[14]		1.7		-:1:-
[6]	110(40)	19(1)	47(5)	6(2):1:2.5(4)
[7]	30	0.4	600	80:1:1600
[8]		0.4		100:1:>100
[17]				100:1:-
Full Wannier model	$\approx 430\gamma$	$\approx 1.8\gamma$	$\approx 600\gamma$	240:1:330
Reduced model		$\approx 2\gamma$		-:1:-

A. Conductivity of the reduced model

The reduced model introduced in Eq. (2) consists of $N_{\mathrm{band}} = 2$ degenerate bands (type A) crossing the Fermi energy dispersing only in the b direction with velocity $v_b^{\mathrm{AA}}(\mathbf{k}) = -\frac{2t_{\mathrm{AA}}}{\hbar} b \sin(k_b b)$ [Eq. (A5)]. In this case of diagonal velocities and spectral functions, the conductivity (see Appendix A1) becomes

$$\begin{aligned}\sigma_{bb} = \frac{16e^2t_{\mathrm{AA}}^2}{\hbar}\frac{b^2}{ac}\int_{-\infty}^{\infty} d\omega \frac{\beta}{2\{1+\cosh[\beta(\omega-\mu)]\}} \\ \times \int_0^{\frac{\pi}{b}} dk_b \sin^2(k_b b)\left(\frac{\gamma}{\pi}\right)^2 \\ \times \frac{1}{\{[\omega - 2t_{\mathrm{AA}}\cos(k_b b)]^2 - \gamma^2\}^2},\end{aligned}$$

where we introduced a phenomenological scattering $\gamma \sim |\mathrm{Im}[\Sigma(\omega = \mu)]|$ in the Lorentzian-shaped spectral function. In the low-temperature small-scattering limit we find

$$\begin{aligned}\sigma_{bb} = \frac{16e^2t_{\mathrm{AA}}^2}{\hbar}\frac{b^2}{ac}\int_{-\infty}^{\infty} d\omega\, \delta(\omega-\mu) \\ \times \int_0^{\frac{\pi}{b}} dk_b \sin^2(k_b b)\frac{\delta[\omega - 2t_{\mathrm{AA}}\cos(k_b b)]}{2\pi\gamma},\end{aligned}$$

which evaluates to

$$\sigma_{bb} = \frac{4e^2}{h\gamma}\frac{b}{ac}\sqrt{(2t_{\mathrm{AA}})^2 - \mu^2} \overset{\mu=0}{\approx} N_{\mathrm{spin}}N_{\mathrm{band}}\frac{D}{R_K\gamma}\frac{b}{ac},$$

with $D = 2t_{\mathrm{AA}}$ and $R_K = \frac{h}{e^2}$ the von Klitzing constant. Using this expression we find for the resistivity $\rho_{bb} = \frac{1}{\sigma_{bb}} \approx 2\gamma$[eV] m Ωcm. Considering a reasonable mean-free path d of the order of a unit-cell length and using the calculated Fermi velocity of $\approx 10^5$ m/s we can estimate a scattering

of $\gamma[\text{eV}] = \frac{0.658}{d[\text{Å}]} \approx 0.05$ eV which implies a resistivity of $\rho_{bb} \approx 0.1$ m Ωcm.

B. Conductivity anisotropy

The reduced model is limited to transport in the b direction. To study the high transport anisotropy suggested by experiments, we calculate the conductivity tensor of the full four-orbital Wannier model. We evaluate Eq. (A1) numerically at $T = 4.2$ K and for small scattering γ (for details see Appendix A2). For the resistivity we obtain $\rho_a \approx 430\gamma$[eV] m Ωcm, $\rho_b \approx 1.8\gamma$[eV] m Ωcm, and $\rho_c \approx 600\gamma$[eV] m Ωcm ($\rho_a : \rho_b : \rho_c \sim 240 : 1 : 330$). Note that the b-axis resistivity in the strictly one-dimensional model (2) is only ≈10% larger than the resistivity in the four-orbital model, which means that the reduced model yields already a quite accurate description of the b-axis transport. The a- and c-axis resistivities are roughly two orders of magnitude larger than in the b direction, compatible with experimental data. Using the same phenomenological scattering $\gamma \approx 0.05$ as motivated in the previous section, we obtain $\rho_a \approx 20$ m Ωcm, $\rho_b \approx 0.1$ m Ωcm, and $\rho_c \approx 30$ m Ωcm. The resistivity ratio of $\rho_a/\rho_b \sim 240$ does compare best to the experimental value 260 as obtained in [5] (see Table I).

IV. CORRELATED ELECTRONIC STRUCTURE

The obtained Wannier model is close to being half-filled which indicates that the local part of the Coulomb interactions is most important. The effects of off-diagonal Coulomb interactions are small and further discussed in Appendix B. In the following, we focus on local electron-electron interactions of density-density type, which are added to the *ab initio* tight-binding Wannier model

$$\hat{\mathcal{H}} = \hat{\mathcal{H}}_{\text{Wannier}} + \hat{\mathcal{H}}_{\text{int}}, \tag{3}$$

where the single-particle part $\hat{\mathcal{H}}_{\text{Wannier}}$ is defined in Eq. (1) and

$$\hat{\mathcal{H}}_{\text{int}} = \sum_{\mathbf{R}} \sum_{\alpha} U_\alpha \hat{n}_{\mathbf{R}\alpha\uparrow} \hat{n}_{\mathbf{R}\alpha\downarrow}, \tag{4}$$

where $\hat{n}_{\mathbf{R}\alpha\sigma}$ is the particle-number operator for Wannier orbital $\alpha = \{\text{A},\text{A}',\text{B},\text{B}'\}$ and spin $\sigma = \{\uparrow, \downarrow\}$ in unit cell $\mathbf{R}$. In order to treat the different band fillings in the model properly, we employ a simple double-counting correction [92] in $\hat{\mathcal{H}}_{\text{Wannier}}$,

$$M^{+\text{DC}}_{\mathbf{0}\alpha\mathbf{0}\alpha} = M_{\mathbf{0}\alpha\mathbf{0}\alpha} - U_\alpha \langle n_{\mathbf{0}\alpha} \rangle_{\text{Wannier}}, \tag{5}$$

where the densities $\langle n \rangle_{\text{Wannier}}$ are taken from the noninteracting Wannier model. Adding interactions we furthermore set the chemical potential μ such that the average filling of electrons in the system is at its physical value $\langle n \rangle \approx 1.44$.

This interacting theory is challenging to solve, even more so because the expected results hint to low-dimensional physics which can promote nonlocal self-energy effects. We employ two complementary techniques to study on a first, more qualitative level, the effect of interactions. First, we apply the VCA, which contains nonlocal contributions to the self-energy Σ. Second, we augment these results by a DMFT calculation which neglects contributions of nonlocal self-energy terms, but is superior in the treatment of the low-energy quasiparticle resonance.

A. Variational cluster approach

The VCA [67] is a quantum many-body cluster method which is capable of treating short-range correlations exactly [65,67,93,94]. The given lattice Hamiltonian is partitioned into a cluster and an intercluster Hamiltonian $\hat{\mathcal{H}} = \hat{\mathcal{H}}^{\text{cl}} + \hat{\mathcal{H}}^{\text{inter}}$, where only single-particle terms are allowed in the intercluster part (for details, see Appendix B). Clusters consist of one or more unit cells and are chosen so that their single-particle Green's function $g^\sigma_{ml}(z)$ can be obtained exactly. We use clusters consisting of two unit cells in the b direction ($L_{\mathcal{C}} = 8$) to capture at least the most basic nonlocal self-energy effects on the quasi-one-dimensional chains which enable signatures of a possible spin-charge separation [66]. In this work, we employ a numerical band Lanczos scheme and the Q-matrix formalism to obtain $g^\sigma_{ml}(z)$ [95]. The CPT approximation to the single-particle Green's function of the full system $G^{-1}(z)$ is given within first-order strong coupling perturbation theory by [63,64]

$$G^{-1}(z) = g^{-1}(z) - H^{\text{inter}}, \tag{6}$$

where H^{inter} are the matrix elements of the intercluster Hamiltonian in the basis of cluster orbitals. If the cluster is larger than the actual unit cell of the crystal, we use a Green's function periodization prescription to project on the original unit cell $G_{\alpha\beta}(z)$ [94].

Within VCA, Eq. (6) is evaluated at the stationary point of the generalized grand potential $\Omega[\mathbf{\Sigma}]$ (for fermions at zero temperature) which is available from G and g [67]. The grand potential is parametrized by the VCA variational parameters $\mathbf{\Delta}$ which are fixed by the VCA condition [67]

$$\nabla_{\mathbf{\Delta}} \Omega(\mathbf{\Delta}) \stackrel{!}{=} \mathbf{0}. \tag{7}$$

The VCA improves the CPT ($\mathbf{\Delta} \equiv \mathbf{0}$) approximation (which is to approximate the self-energy Σ_G of the full system by the self-energy of the cluster Σ_g) by adding flexibility to the cluster self-energy in terms of variational parameters $\mathbf{\Delta}$. We consider the onsite energies of the four Wannier orbitals as independent variational parameters $\mathbf{\Delta} = \{\Delta_{\epsilon_{\text{A}}}, \Delta_{\epsilon_{\text{A}'}}, \Delta_{\epsilon_{\text{B}}}, \Delta_{\epsilon_{\text{B}'}}\}$ (which implicitly includes an overall shift of the chemical potential of the cluster) and use $N_{1.\text{BZ}} = 32^3$ k points in the irreducible BZ for the evaluation of Eq. (7).

Advantages of the VCA are that (i) it is exact in the noninteracting system, (ii) the approximation is systematically improvable by enlarging cluster sizes, (iii) or increasing the number of variational parameters $\mathbf{\Delta}$, and (iv) it is possible to work directly in the real energy domain as well as in Matsubara space. VCA on small clusters is inherently biased towards the insulating state, therefore we expect to overestimate a possible Mott gap (see Appendix C for a discussion).

B. Dynamical mean field theory

A complementary approach that neglects nonlocal effects but describes the local dynamical quantum fluctuations better is the DMFT [96]. Within this theory, the interacting lattice problem is mapped on a self-consistent four-orbital impurity model coupled to an infinite electronic bath. The DMFT approximation is to assume a momentum-independent

self-energy of the original model $\Sigma_{\alpha\beta}$:

$$\Sigma_{\alpha\beta}(i\omega,\mathbf{k}) \stackrel{!}{=} \mathcal{S}_{\alpha\beta}(i\omega),$$

where $\mathcal{S}_{\alpha\beta}$ is the local self-energy generated by the auxiliary quantum impurity system.

As impurity solver we use the continuous time quantum Monte Carlo (CT-QMC) code of the TRIQS [97] toolkit and its implementation of the hybridization expansion (CT-HYB) [98,99] algorithm using Legendre polynomials [100]. This sign-problem free method works in Matsubara space and provides statistically exact and reliable results even at very low temperatures [101]. We used a low temperature of $\beta = 150\ \mathrm{eV}^{-1}$ and a k mesh of $N_{1.\mathrm{BZ}} = 800$. The imaginary-time data are continued to the real-frequency axis using a parallel tempering analytic continuation method [102].

Different to VCA, the DMFT as applied here neglects nonlocal correlations. On the other hand, it treats the local dynamical quantum fluctuations accurately.

C. Discussion of the interacting dynamics

For models based on *atomic* orbitals, constrained LDA calculations suggest an onsite interaction for the atomic d Mo orbitals of $U \approx 6.4$ eV and a nearest-neighbor interaction of $V \approx 0.2$ eV [52] in $Li_{0.9}Mo_6O_{17}$, while the bulk Mo value for the onsite interaction is $U \approx 3.8$ eV [48]. As we will discuss in the following, in our model these larger interaction values U, which have been proposed and used for model calculations [48,49], do not give results in accordance with experimental data. Obtaining the interaction parameters in an *ab initio* way by, e.g., the constrained random phase approximation (cRPA) [61,103], would be highly desirable, but is beyond our present computational capabilities due to the very large unit cell of the system.

In the following, based on physical arguments, we will nevertheless argue that a moderate value of U is appropriate for our model. We use uniform *onsite* interactions $U_\alpha = U$ only and estimate the magnitude of the interaction strength to be of the order of a few $t_{\max}$. The reduced value, compared to the atomic one, can be motivated by (i) the large spread of the orbitals [104] and (ii) the effective screening of other Mo $4d$ states near the Fermi level. We want to remind the reader that we are not dealing with atomic orbitals (where for molybdenum the interaction U could be of the order of several electron volts) but with extended, even molecularlike, orbitals (see Fig. 4).

Let us start the discussion using interaction values of the order of the bandwidth, i.e., using $U = 1$ eV. We show results for the single-particle spectrum and orbitally resolved DOS of the interacting model in Figs. 6 (left and center) and 7 [105]. We used a Lorentzian broadening of $0^+ = 0.05$ eV for plotting the spectral functions, as well as $0^+ = 0.025$ eV for plotting the DOS. As discussed in the previous section, the VCA is biased towards an insulating solution (see also Appendix C), that is why there is a small gap in the conduction band visible in the spectral function, which is not seen in the DMFT results.

Comparing the single-particle dynamics to recent experiments (ARPES data from Refs. [21,22]), we find very good agreement for the bands at the Fermi energy (Fig. 6, right). The renormalization of the effective mass of the half-filled orbitals, calculated from the DMFT self-energy, is $m \approx 1.2 m_0$, where m_0 is the LDA band mass.

Regarding the bands crossing the Fermi energy, their slope improves in VCA/DMFT with respect to the LDA data,

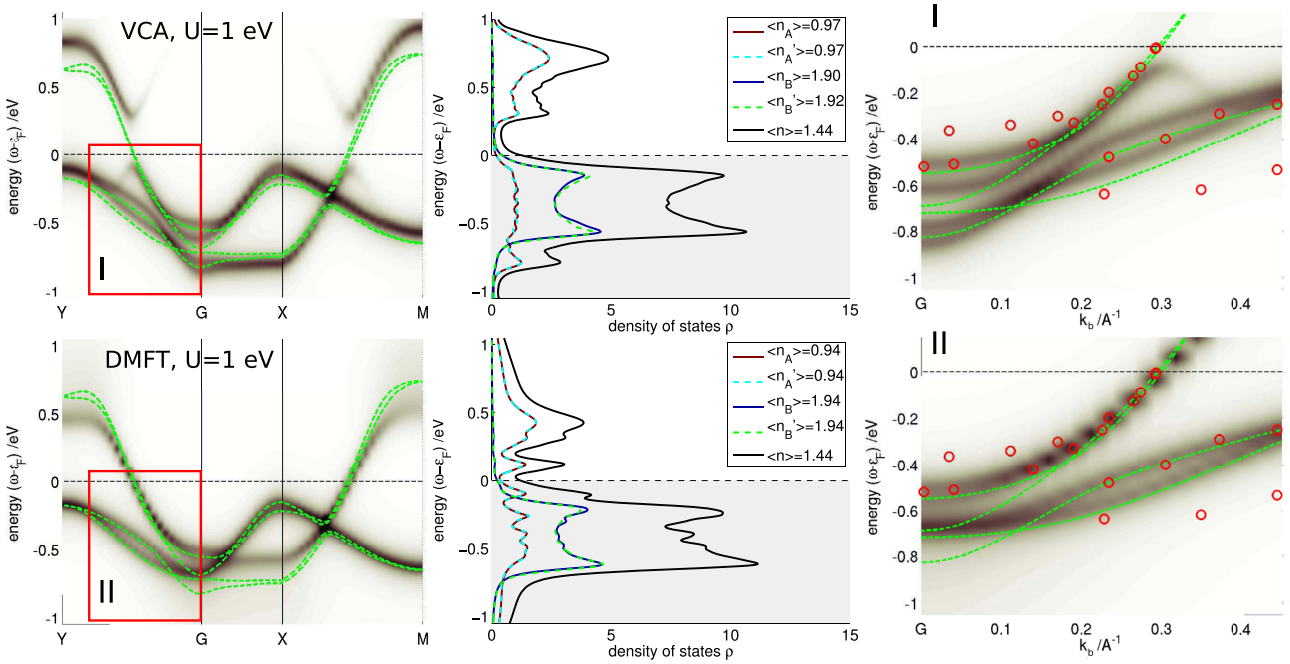

FIG. 6. (Color online) Spectral function and DOS of the interacting model. Top row: VCA data for $U = 1$ eV using eight-orbital clusters. Bottom row: DMFT data for $U = 1$ eV. Left: Spectral function plotted along a two-dimensional path in the reciprocal b-c plane. The noninteracting dispersion is plotted on top (dashed green line). Center: Orbitally resolved density of states. Right: Zoom to the spectral function in the respective red rectangle compared to ARPES data from Ref. [22] which are indicated as red circles.

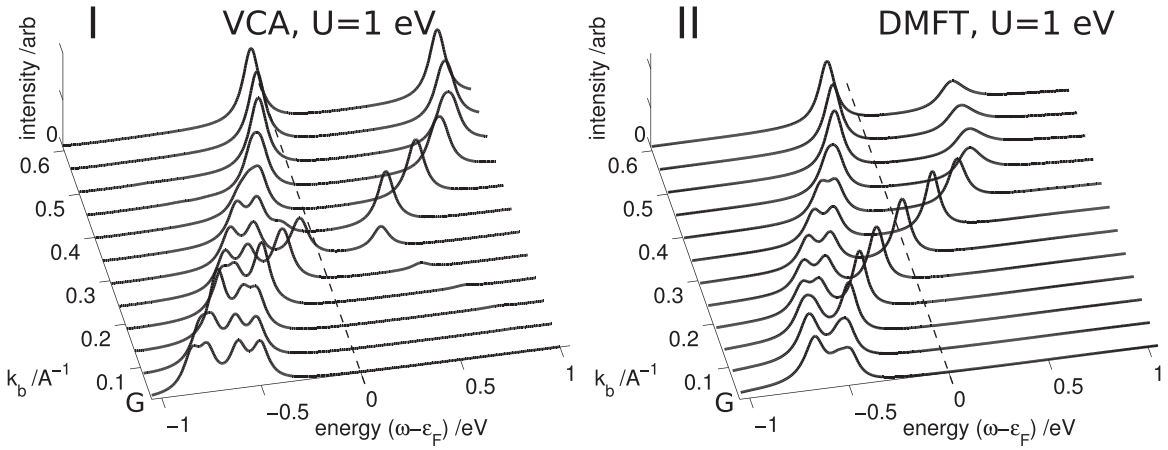

FIG. 7. Cuts through the spectral function along the b axis. The parameters and labels (I, II) correspond to those in Fig. 6.

and compares well with the measured excitations in ARPES experiments [22]. Note that the upmost branch provides only a very weak signal in the ARPES data as compared to the lower branch. In our DMFT calculation, the electronic correlations suppress the hybridizations between chains A and A′, making them equivalent. This leads to only one dispersing feature crossing the Fermi energy (see Fig. 6, lower right panel). The red circles at lower binding energy correspond to the shoulder in the ARPES data, which are very likely due to nonlocal correlation effects that are completely neglected in the single-site DMFT approach. A final statement on the impact of nonlocality of the self-energy and spin-charge separation on the single-particle excitations requires a detailed investigation on large systems, which is beyond the scope of this paper.

Increasing the interaction value further, for instance to $U = 1.5$ eV, does not change results significantly (left aside the artificial gap in the VCA calculation). Above a certain limit, however, which is around $U = 2.5$ eV in our calculations, a Mott gap opens in the two half-filled bands. An extreme example is using the atomic value for the interaction $U = 6$ eV, which is shown in Fig. 8. The half-filled bands are in the Mott insulating state, with the spectral weight transferred to roughly ± 3 eV. The only spectral weight left close to the Fermi level originates from the two almost filled orbitals, type B. This is of course qualitatively different from experimental results.

The values of U given here can only be seen as rough estimates to the actual value, and are by no means *ab initio*. The DMFT overestimates the metallicity of a system, in particular in low dimensions, while the VCA underestimates it. Hence, using different techniques which are tailored more towards low dimensions, the needed value of U to open a Mott gap might be even smaller. As has been shown by Chudzinski *et al.* [48], the system should be metallic, but very close to an insulating state. Our observations can be used as a guideline in further studies to determine the value of U. At very large coupling $U = 6$ eV, however, the system as modeled here is strongly localized, and the insulating state there should be very robust. This is supported by the fact that both methods, VCA and DMFT, give indistinguishable results in this (almost) atomic limit. It clearly shows that taking atomic values

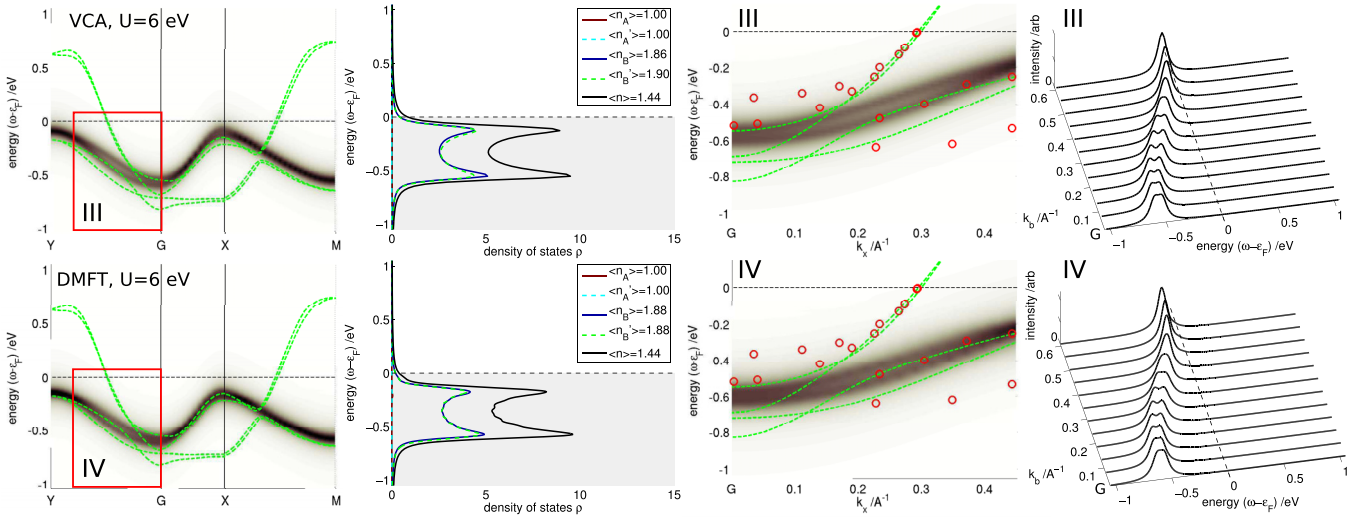

FIG. 8. (Color online) Spectral function and DOS of the interacting model for high values of onsite interaction strength as one would expect for atomiclike molybdenum d orbitals: $U = 6$ eV. For legends, arrangement of the subplots, and color coding, see Fig. 6. On the far right we show cuts through the spectral function as in Fig. 7.

for U is inadequate for the effective model derived in this work.

Let us shortly comment on the effect of correlations in the reduced model (Sec. II C). There, the Hamiltonian of the half-filled and the filled bands decouples exactly, which means that one is left with a standard one-dimensional (almost) half-filled Hubbard model with nearest-neighbor hopping only [106]. As discussed in Secs. II C and III A, this gives a quite good description of the dispersion in chain direction including transport properties. Effects beyond the one-dimensional Hubbard model can be included using the effective perpendicular hopping terms as estimated in Sec. II C. In a recent study on dimensional crossover [40], the critical perpendicular coupling to enter the regime of one-dimensional physics is $t_p \approx 0.18t$ at interaction strength $U = 3t$. Of course, this value depends on model details such as frustrated hopping and interaction strength. However, since our estimated value for t_p in $Li_{0.9}Mo_6O_{17}$ is significantly smaller than this boundary, we suggest that this can explain the robustness of one-dimensional (1D) physics in this compound. We leave a more detailed study of the dimensional crossover in $Li_{0.9}Mo_6O_{17}$ for further investigations.

V. CONCLUSIONS

We have devised a model for the electronic structure of the highly anisotropic low-dimensional purple bronze $Li_{0.9}Mo_6O_{17}$. Starting from *ab initio* calculations, applying density functional theory in the local density approximation, we constructed a four-orbital model based on molybdenum d states in terms of maximally localized Wannier functions. This leads to an effective theory with *two filled bands* slightly below and *two half-filled bands* crossing the Fermi energy. We obtained an even more elementary effective model with reduced dimensionality consisting of two orbitals only, tailored towards studies of interactions at low energies.

We showed that basic electronic properties of our model are in good agreement with experimental data and *ab initio* results. Estimated anisotropic transport coefficients reproduce experimental trends. The model enables us to study effects of many-body correlations. In a first approach, we made use of the (extended) variational cluster approach which takes into account nonlocal contributions to the self-energy and dynamical mean field theory to study the effects of density-density type electron-electron interactions. Our results indicate that moderate onsite interactions (of the order of the bandwidth) are essential, while nearest-neighbor density-density interactions play a minor role. The so-obtained single-particle spectra agree well with recent angle-resolved photoemission experiments. Our study sets some qualitative limits on the value of the interaction parameters. In particular, we could show that the values used for atomiclike molybdenum d orbitals are completely inappropriate for our Wannier model of lithium purple bronze.

We would like to point out that our model is very different from previously proposed descriptions for $Li_{0.9}Mo_6O_{17}$ which were based on atomic orbitals with a comparatively high onsite interaction strength of several electron volts. We suggest that low-energy treatments of this one-dimensional model should start from two half-filled chains with moderate onsite interaction rather than quarter-filled ladder models with high values of onsite interaction strength plus off-diagonal interactions.

Our model is intended to serve as a starting point for future studies of the electronic structure and interactions of $Li_{0.9}Mo_6O_{17}$ be it in a renormalization group Luttinger liquid or computational many-body sense. On the latter side it would certainly be interesting to conduct a more thorough investigation of nonlocal self-energy effects to complement our (extended) variational cluster approach results. In particular, the phenomenon of spin-charge separation deserves further attention. A theoretical understanding of the phase diagram of the system, i.e., the occurrence of superconducting, insulating, or charge ordered states as function of pressure and temperature, remains a challenging open question. These studies could be augmented by an *ab initio* calculation of interaction parameters for the Wannier model by appropriate techniques such as constrained random phase approximation [61,103], making the approach fully *ab initio*. At the moment of writing, this is not feasible due to the computational complexity.

ACKNOWLEDGMENTS

We gratefully acknowledge fruitful discussions with J. W. Allen, W. von der Linden, E. Arrigoni, C. Heil, J. Mravlje, F. Assaad, and in particular P. Chudzinski. M.N. thanks the Forschungszentrum Jülich-Autumn School on Correlated Electrons for hospitality. This work was partly supported by the Austrian Science Fund (FWF) P24081-N16 and SFB-ViCoM subprojects F04103, and some calculations have been performed on the Vienna Scientific Cluster (VSC).

APPENDIX A: LINEAR RESPONSE TRANSPORT

The structure of the conductivity tensor $\sigma_{\alpha\beta}$ of $Li_{0.9}Mo_6O_{17}$ follows from the C_{2h} point symmetry as well as physical symmetry considerations for the conductivity [107] and can easily be established by requiring the conductivity tensor to be (i) symmetric for physical reasons and (ii) invariant under transformations with the four lattice point symmetry operations (identity, inversion, mirror symmetry perpendicular to the a axis and twofold rotation around the a axis) S_α: $\sigma = S_\alpha \sigma S_\alpha^T$.

1. Formalism

Following Refs. [108–110], linear response transport coefficients can be expressed in terms of kinetic coefficients

$$\mathcal{A}^n_{\nu\mu} = N_{\text{spin}} \pi \hbar \int_{-\infty}^{\infty} d\omega \, (\beta\omega)^n \times p_{\text{FD}}(\omega,\mu,\beta) p_{\text{FD}}(-\omega,-\mu,\beta) \Gamma_{\nu\mu}(\omega,\omega), \quad \text{(A1)}$$

where $N_{\text{spin}} = 2$ is due to spin degeneracy, the indices $\nu,\mu = \{a,b,c\}$ denote the real-space coordinate system, and we neglect vertex corrections. The Fermi-Dirac distribution $p_{\text{FD}}(\omega,\mu,\beta) = \frac{1}{e^{\beta(\omega-\mu)}+1}$ restricts the interval of integration to $\beta^{-1} \sim k_B T$ around the Fermi energy ϵ_F (k_B is Boltzmann's constant, and T and β denote temperature and inverse

temperature, respectively). The transport distribution

$$\Gamma_{\nu\mu}(\omega_1,\omega_2) = \frac{1}{V}\frac{1}{N_{1.\mathrm{BZ}}}\sum_{\mathbf{k}\in 1.\mathrm{BZ}} \mathrm{Tr} \times [v_\nu(\mathbf{k})A(\omega_1,\mathbf{k})v_\mu(\mathbf{k})A(\omega_2,\mathbf{k})] \quad \text{(A2)}$$

($V = abc$ is the unit-cell volume) is given in terms of the velocities

$$v_\nu^{\alpha\beta}(\mathbf{k}) = -\frac{\hbar}{m}\langle\Psi_\alpha(\mathbf{k})|\,\nabla_\nu\,|\Psi_\beta(\mathbf{k})\rangle \quad \text{(A3)}$$

and the spectral function

$$A_{\alpha\beta}(\omega,\mathbf{k}) = -\frac{1}{\pi}\mathrm{Im}\left[G^R_{\alpha\beta}(\omega,\mathbf{k})\right], \quad \text{(A4)}$$

which both are matrices in orbital indices $\alpha,\beta = \{\mathrm{A},\mathrm{A}',\mathrm{B},\mathrm{B}'\}$, which the trace Tr runs over.

We use velocities $v_\nu^{\alpha\beta}(\mathbf{k})$ [Eq. (A3)] in the Peierls approximation (neglecting the gradient of the Wannier orbital itself leading to a diagonal representation)

$$v_\nu^{\alpha\beta}(\mathbf{k}) = \frac{1}{\hbar}\Bigg(\langle\omega_\alpha(\mathbf{k})|\,\frac{\partial\hat{\mathcal{H}}(\mathbf{k})}{\partial k_\nu}\,|\omega_\beta(\mathbf{k})\rangle - \alpha(r_\alpha - r_\beta)\,\langle\omega_\alpha(\mathbf{k})|\,\hat{\mathcal{H}}(\mathbf{k})\,|\omega_\beta(\mathbf{k})\rangle\Bigg) \approx \frac{1}{\hbar}\frac{\partial E_\alpha(\mathbf{k})}{\partial k_\nu}\delta_{\alpha\beta}, \quad \text{(A5)}$$

where the second term in the first expression takes intra-unit-cell processes into account [109] and r_α is the position of Wannier orbital α inside the unit cell. This term is neglected in the following because the intra-unit-cell hopping elements are negligibly small. The conductivity tensor is

$$\sigma_{\nu\mu} = \beta e^2 \mathcal{A}^0_{\nu\mu}, \quad \text{(A6)}$$

with e denoting the electron charge.

2. Details on the evaluation of the anisotropic conductivity

In this appendix, we outline the numerical procedure used for the evaluation of the conductivity tensor (A6). These equations contain four additional, auxiliary numerical parameters in which we converge our results: (i) The spectral function $A_{\alpha\beta}(\omega,\mathbf{k})$ [Eq. (A4)] of the Wannier Hamiltonian is available exactly through the noninteracting retarded single-particle Green's function $G^R_{\alpha\beta}(\omega) = \langle\omega_\alpha(\mathbf{k})|\,\frac{1}{\omega+i\gamma-\hat{\mathcal{H}}(\mathbf{k})}\,|\omega_\beta(\mathbf{k})\rangle$. The broadening γ of the spectral function is chosen phenomenologically as described in the main part of the text. For numerical reasons, γ has to be chosen in accordance with (ii) the number of k points $N_{1.\mathrm{BZ}}$ in the first BZ for the sum in Eq. (A2). We obtain converged conductivities for $N_{1.\mathrm{BZ}}^{1/3} \in [1,67]$ to within a relative error of 10^{-3} using an equidistant grid in the irreducible BZ. We use $\gamma = \{0.1,0.075,0.05,0.025\}$ and rescale all conductivities with γ. As a function of γ, the resistivities in the a and b directions are constant at $\rho_a \approx (1.8 \pm 0.05)\gamma$ and $\rho_b \approx (430 \pm 10)\gamma$, while the resistivity in the c direction shows an upward trend. For our values of γ we find $\rho_c \approx \{190,300,480,650\}\gamma$. Since the last data point at $\gamma = 0.025$ is already difficult to converge in $N_{1.\mathrm{BZ}}$, we estimate $\rho_c \approx (600 \pm 150)\gamma$.

(iii) The velocities $v_\nu^{\alpha\beta}(\mathbf{k})$ [Eq. (A3)] are obtained by symmetric first-order numeric gradient approximations $v_\nu^{\alpha\beta}(\mathbf{k}) \approx \frac{\delta_{\alpha\beta}}{\hbar}\frac{E_\alpha(\mathbf{k}+\frac{\delta}{2}\mathbf{e}_\nu)-E_\alpha(\mathbf{k}-\frac{\delta}{2}\mathbf{e}_\nu)}{\delta}$ ($\mathbf{e}_\nu$ denotes the unit vector in real-space dimension ν). The parameter of the finite-difference scheme for the velocities used is $\delta = 10^{-6}$ after finding only negligible changes in a range of $\delta \in [10^{-8},10^{-3}]$. (iv) For reasons of numerical stability, we evaluate Eq. (A6) at a low, but finite temperature of $T = 4.2$ K, keeping in mind that $v_\nu^{ij}(\mathbf{k})$ and $A(\omega,\mathbf{k})$ have been evaluated for zero temperature. We find the results to be independent of this choice in a range of $T \in [1,50]$ K. In this calculation, at fixed γ, the temperature dependence enters through the Fermi-Dirac distribution only and a small scattering is taken into account through the broadening γ in the spectral function. We checked the numeric procedure on the reduced model where analytic results are known (see main text).

APPENDIX B: NONLOCAL INTERACTIONS: EXTENDED VCA

Here, we outline the VCA theory as implemented to obtain the results of the main text including the extensions needed in eVCA to treat nonlocal Coulomb interactions [65]. The single-particle part of the full Hamiltonian is readily decomposed into a cluster and an intercluster part

$$\hat{\mathcal{H}}^{\mathrm{cl}}_{\mathrm{Wannier}} = M_{\boldsymbol{\mathcal{R}}m\boldsymbol{\mathcal{R}}l}\,|\omega_m\rangle\,\langle\omega_l|\,,$$
$$\hat{\mathcal{H}}^{\mathrm{inter}}_{\mathrm{Wannier}} = \sum_{\delta\mathcal{R}} e^{-i\mathbf{k}\cdot\delta\mathcal{R}} M_{\boldsymbol{\mathcal{R}}m\boldsymbol{\mathcal{R}}'l}\,|\omega_m\rangle\,\langle\omega_l|\,,$$

where indices m and l run over the $L_\mathcal{C}$ orbitals in the cluster $\mathcal{C}$ at superlattice [94] position $\boldsymbol{\mathcal{R}}$.

When off-diagonal interaction terms are nonzero, an additional mean field treatment is needed for those two-particle terms which extend over the cluster boundary [65]. This leads to a modified interaction part of the Hamiltonian

$$\hat{\mathcal{H}}_{\mathrm{int}} = \sum_{\mathcal{C}}\left(\hat{\mathcal{H}}^{\mathrm{cl}}_{\mathrm{int}} + \hat{\mathcal{H}}^{\mathrm{cl}}_{\mathrm{mf}}(\boldsymbol{\varphi})\right),$$

$$\hat{\mathcal{H}}^{\mathrm{cl}}_{\mathrm{int}} = \sum_{m=1}^{L_\mathcal{C}} U_m\,\hat{n}_{m\uparrow}\hat{n}_{m\downarrow} + \sum_{\substack{m<l\in\mathcal{C}\\ \sigma\sigma'}} V_{ml}\,\hat{n}_{m\sigma}\hat{n}_{l\sigma'},$$

$$\hat{\mathcal{H}}^{\mathrm{cl}}_{\mathrm{mf}}(\boldsymbol{\varphi}) = \sum_{ml}\widetilde{V}_{ml}\left(\sum_\sigma(\hat{n}_{m\sigma}\varphi_l + \hat{n}_{l\sigma}\varphi_m) - \varphi_l\varphi_m\right),$$

with onsite interaction strength U_m, intracluster off-diagonal interactions V_{ml}, as well as $\widetilde{V}_{ml} = \sum_{\boldsymbol{\mathcal{R}}} V_{0m\boldsymbol{\mathcal{R}}l}$ the interaction elements in the mean field Hamiltonian. The mean fields $\boldsymbol{\varphi}$ (taken as spin independent $\varphi_m = \sum_\sigma\langle\hat{n}_{m\sigma}\rangle$ and restricted by lattice symmetry) need to be determined self-consistently.

This allows us to write the (interacting) cluster Hamiltonian in the VCA as

$$\hat{\mathcal{H}}^{\mathrm{cl}}(\boldsymbol{\Delta},\boldsymbol{\varphi}) = \hat{\mathcal{H}}^{\mathrm{cl}}_{\mathrm{Wannier}}(\boldsymbol{\Delta}) + \hat{\mathcal{H}}^{\mathrm{cl}}_{\mathrm{int}} + \hat{\mathcal{H}}^{\mathrm{cl}}_{\mathrm{mf}}(\boldsymbol{\varphi}),$$

where we introduced the VCA variational parameters [67,93] $\boldsymbol{\Delta}$.

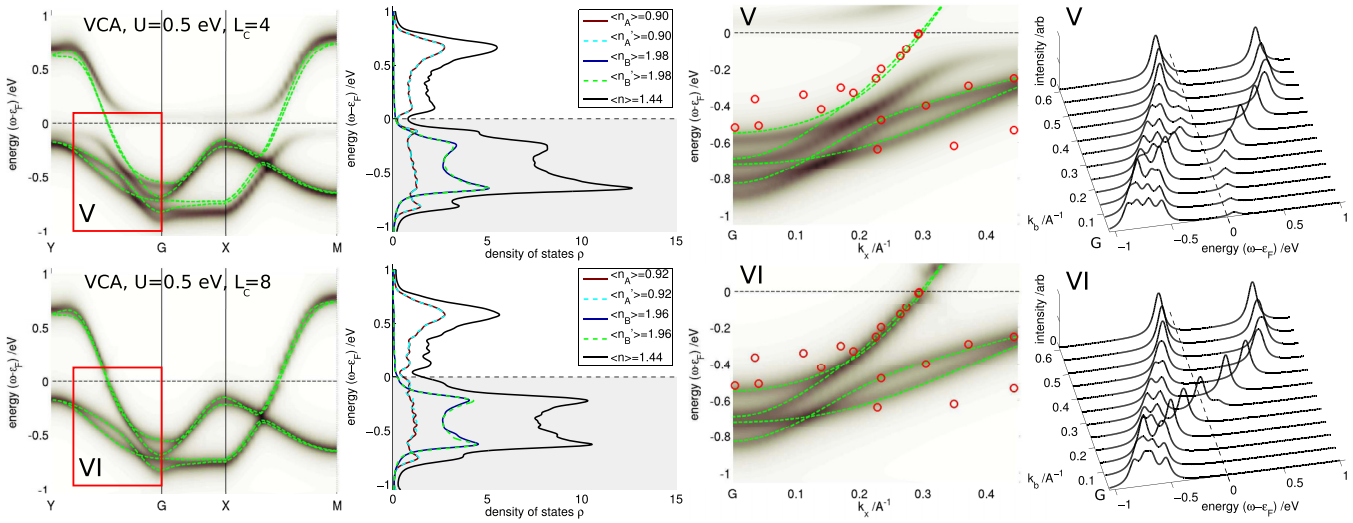

FIG. 9. (Color online) Comparison of VCA cluster sizes for a moderate onsite interaction strength of $U = 0.5$ eV. Top row: VCA data for using four-orbital clusters. Bottom row: VCA data for using eight-orbital clusters. For legends, arrangement of the subplots, and color coding, see Fig. 8.

To study the impact of nonlocal Coulomb interactions, we extend Eq. (4) by

$$\hat{\mathcal{H}}_{\text{int,nl}} = \hat{H}_{\text{int}} + \sum_{\mathbf{R}<\mathbf{R}'} \sum_{\substack{\alpha<\beta \\ \sigma\sigma'}} V_{\mathbf{R}\alpha\mathbf{R}'\beta}\, \hat{n}_{\mathbf{R}\alpha\sigma} \hat{n}_{\mathbf{R}'\beta\sigma'},$$

which also effects the double-counting terms in Eq. (5)

$$M^{\text{+DC,nl}}_{\mathbf{0}\alpha\mathbf{0}\alpha} = M^{\text{+DC}}_{\mathbf{0}\alpha\mathbf{0}\alpha} - \sum_{\mathbf{R}\gamma} V_{\mathbf{0}\alpha\mathbf{R}\gamma} \langle n_{\mathbf{R}\gamma} \rangle_{\text{Wannier}},$$

where the sum over $(\mathbf{R},\gamma)$ runs over all bonds connected to orbital $(\mathbf{0},\alpha)$. The mean fields $\boldsymbol{\varphi}$ [65] which arise due to off-diagonal interaction terms are fixed by the eVCA condition on the generalized grand potential [111]

$$\nabla_{\boldsymbol{\Delta},\boldsymbol{\varphi}} \Omega(\boldsymbol{\Delta},\boldsymbol{\varphi}) \stackrel{!}{=} \mathbf{0}.$$

In order to check the influence of *nearest-neighbor density-density interactions* $V_{\mathbf{R}\alpha\mathbf{R}'\beta}$, we did several eVCA calculations with different values within reasonable limits, i.e., below a value of $\approx \frac{U}{2}$. Our calculations show, however, that these interactions $V_{\mathbf{R}\alpha\mathbf{R}'\beta}$ lead only to minor differences compared to results without them. We did not find the system to be susceptible to any charge ordering. For that reason, and also because the precise value of the parameters $V_{\mathbf{R}\alpha\mathbf{R}'\beta}$ is complicated to estimate, all results presented here are calculated with onsite interaction $U_\alpha = U$ only [112]. Given the band-filling factors and the good agreement with ARPES experiments, we argue that onsite interactions are sufficient to describe the spectral properties of this system within our approximation.

APPENDIX C: VCA CLUSTER SIZE EXTRAPOLATION

Here, we discuss the approximation introduced by choosing eight-orbital clusters for the VCA procedure. Eight-orbital clusters enable nonlocal self-energy effects along the chain direction in the most basic fashion. The VCA on small cluster sizes is inherently biased towards the insulating state [94]. In Fig. 9, we show the behavior of the results when going from one-unit-cell clusters $L_\mathcal{C} = 4$ to two-unit-cell clusters in the b direction $L_\mathcal{C} = 8$. For the same interaction strength, the $L_\mathcal{C} = 4$ calculation clearly shows a pronounced Mott gap in the A-type orbitals while it is still absent in the $L_\mathcal{C} = 8$ calculation. All other basic features are comparable. For numerical reasons, we can not go to larger cluster sizes. Nevertheless, we expect the results of the $L_\mathcal{C} = 8$ calculation to be still heavily biased towards the insulating state. One can regard the critical value $U \approx 0.7$ eV for which the gap opens at $L_\mathcal{C} = 8$ as a lower bound to the true critical interaction.

[1] W. McCarroll and M. Greenblatt, J. Solid State Chem. **54**, 282 (1984).
[2] M. Greenblatt, Chem. Rev. **88**, 31 (1988).
[3] M. Onoda, K. Toriumi, Y. Matsuda, and M. Sato, J. Solid State Chem. **66**, 163 (1987).
[4] M. S. da Luz, J. J. Neumeier, C. A. M. dos Santos, B. D. White, H. J. I. Filho, J. B. Leão, and Q. Huang, Phys. Rev. B **84**, 014108 (2011).
[5] M. Greenblatt, W. McCarroll, R. Neifeld, M. Croft, and J. Waszczak, Solid State Commun. **51**, 671 (1984).
[6] M. S. da Luz, C. A. M. dos Santos, J. Moreno, B. D. White, and J. J. Neumeier, Phys. Rev. B **76**, 233105 (2007).
[7] J.-F. Mercure, A. F. Bangura, X. Xu, N. Wakeham, A. Carrington, P. Walmsley, M. Greenblatt, and N. E. Hussey, Phys. Rev. Lett. **108**, 187003 (2012).
[8] X. Xu, A. F. Bangura, J. G. Analytis, J. D. Fletcher, M. M. J. French, N. Shannon, J. He, S. Zhang, D. Mandrus, R. Jin *et al.*, Phys. Rev. Lett. **102**, 206602 (2009).
[9] C. A. M. dos Santos, M. S. da Luz, Y.-K. Yu, J. J. Neumeier, J. Moreno, and B. D. White, Phys. Rev. B **77**, 193106 (2008).

[10] Y. Matsuda, M. Sato, M. Onoda, and K. Nakao, J. Phys. C: Solid State Phys. **19**, 6039 (1986).

[11] C. E. Filippini, J. Beille, M. Boujida, J. Marcus, and C. Schlenker, Phys. C (Amsterdam) **162–164, Part 1**, 427 (1989).

[12] H. Chen, J. J. Ying, Y. L. Xie, G. Wu, T. Wu, and X. H. Chen, Europhys. Lett. **89**, 67010 (2010).

[13] C. A. M. dos Santos, B. D. White, Y.-K. Yu, J. J. Neumeier, and J. A. Souza, Phys. Rev. Lett. **98**, 266405 (2007).

[14] J. Choi, J. L. Musfeldt, J. He, R. Jin, J. R. Thompson, D. Mandrus, X. N. Lin, V. A. Bondarenko, and J. W. Brill, Phys. Rev. B **69**, 085120 (2004).

[15] L. Degiorgi, P. Wachter, M. Greenblatt, W. H. McCarroll, K. V. Ramanujachary, J. Marcus, and C. Schlenker, Phys. Rev. B **38**, 5821 (1988).

[16] J. L. Cohn, B. D. White, C. A. M. dos Santos, and J. J. Neumeier, Phys. Rev. Lett. **108**, 056604 (2012).

[17] N. Wakeham, A. F. Bangura, X. Xu, J.-F. Mercure, M. Greenblatt, and N. E. Hussey, Nat. Commun. **2**, 1 (2011).

[18] M. Boujida, C. Escribe-Filippini, J. Marcus, and C. Schlenker, Phys. C (Amsterdam) **153–155, Part 1**, 465 (1988).

[19] J. Chakhalian, Z. Salman, J. Brewer, A. Froese, J. He, D. Mandrus, and R. Jin, Phys. B (Amsterdam) **359–361**, 1333 (2005).

[20] J. D. Denlinger, G.-H. Gweon, J. W. Allen, C. G. Olson, J. Marcus, C. Schlenker, and L.-S. Hsu, Phys. Rev. Lett. **82**, 2540 (1999).

[21] F. Wang, J. V. Alvarez, S.-K. Mo, J. W. Allen, G.-H. Gweon, J. He, R. Jin, D. Mandrus, and H. Hochst, Phys. Rev. Lett. **96**, 196403 (2006).

[22] F. Wang, J. V. Alvarez, J. W. Allen, S.-K. Mo, J. He, R. Jin, D. Mandrus, and H. Hochst, Phys. Rev. Lett. **103**, 136401 (2009).

[23] G.-H. Gweon, J. W. Allen, and J. D. Denlinger, Phys. Rev. B **68**, 195117 (2003).

[24] G.-H. Gweon, S.-K. Mo, J. W. Allen, J. He, R. Jin, D. Mandrus, and H. Hochst, Phys. Rev. B **70**, 153103 (2004).

[25] F. Wang, J. Alvarez, S.-K. Mo, J. Allen, G.-H. Gweon, J. He, R. Jin, D. Mandrus, and H. Hochst, Phys. B (Amsterdam) **403**, 1490 (2008).

[26] L. Dudy, J. D. Denlinger, J. W. Allen, F. Wang, J. He, D. Hitchcock, A. Sekiyama, and S. Suga, J. Phys.: Condens. Matter **25**, 014007 (2013).

[27] G.-H. Gweon, J. Denlinger, C. Olson, H. Hochst, J. Marcus, and C. Schlenker, Phys. B (Amsterdam) **312–313**, 584 (2002).

[28] G.-H. Gweon, J. D. Denlinger, J. W. Allen, C. G. Olson, H. Höechst, J. Marcus, and C. Schlenker, Phys. Rev. Lett. **85**, 3985 (2000).

[29] J. Hager, R. Matzdorf, J. He, R. Jin, D. Mandrus, M. A. Cazalilla, and E. W. Plummer, Phys. Rev. Lett. **95**, 186402 (2005).

[30] T. Podlich, M. Klinke, B. Nansseu, M. Waelsch, R. Bienert, J. He, R. Jin, D. Mandrus, and R. Matzdorf, J. Phys.: Condens. Matter **25**, 014008 (2013).

[31] T. Giamarchi, Chem. Rev. **104**, 5037 (2004).

[32] M. Pustilnik, M. Khodas, A. Kamenev, and L. I. Glazman, Phys. Rev. Lett. **96**, 196405 (2006).

[33] M. Khodas, M. Pustilnik, A. Kamenev, and L. I. Glazman, Phys. Rev. B **76**, 155402 (2007).

[34] V. Meden and K. Schönhammer, Phys. Rev. B **46**, 15753 (1992).

[35] J. Voit, Phys. Rev. B **47**, 6740 (1993).

[36] G. León, C. Berthod, and T. Giamarchi, Phys. Rev. B **75**, 195123 (2007).

[37] J. Xue, L.-C. Duda, K. E. Smith, A. V. Fedorov, P. D. Johnson, S. L. Hulbert, W. McCarroll, and M. Greenblatt, Phys. Rev. Lett. **83**, 1235 (1999).

[38] S. Biermann, A. Georges, A. Lichtenstein, and T. Giamarchi, Phys. Rev. Lett. **87**, 276405 (2001).

[39] C. Berthod, T. Giamarchi, S. Biermann, and A. Georges, Phys. Rev. Lett. **97**, 136401 (2006).

[40] M. Raczkowski and F. F. Assaad, Phys. Rev. Lett. **109**, 126404 (2012).

[41] C. Schlenker, H. Schwenk, C. Escribe-Filippini, and J. Marcus, Physica B + C (Amsterdam) **135**, 511 (1985).

[42] Y. Matsuda, M. Onoda, and M. Sato, Physica B + C (Amsterdam) **143**, 243 (1986).

[43] T. Ekino, J. Akimitsu, Y. Matsuda, and M. Sato, Solid State Commun. **63**, 41 (1987).

[44] J.-F. Mercure, A. F. Bangura, X. Xu, N. Wakeham, A. Carrington, P. Walmsley, M. Greenblatt, and N. E. Hussey, arXiv:1203.6672.

[45] M. Sato, Y. Matsuda, and H. Fukuyama, J. Phys. C: Solid State Phys. **20**, L137 (1987).

[46] G.-H. Gweon, J. Denlinger, J. Allen, R. Claessen, C. Olson, H. Hochst, J. Marcus, C. Schlenker, and L. Schneemeyer, J. Electron Spectrosc. Relat. Phenom. **117–118**, 481 (2001).

[47] J. Dumas and C. Schlenker, Int. J. Mod. Phys. B **07**, 4045 (1993).

[48] P. Chudzinski, T. Jarlborg, and T. Giamarchi, Phys. Rev. B **86**, 075147 (2012).

[49] J. Merino and R. H. McKenzie, Phys. Rev. B **85**, 235128 (2012).

[50] J. L. Cohn, P. Boynton, J. S. Triviño, J. Trastoy, B. D. White, C. A. M. dos Santos, and J. J. Neumeier, Phys. Rev. B **86**, 195143 (2012).

[51] M. H. Whangbo and E. Canadell, J. Am. Chem. Soc. **110**, 358 (1988).

[52] Z. S. Popović and S. Satpathy, Phys. Rev. B **74**, 045117 (2006).

[53] T. Jarlborg, P. Chudzinski, and T. Giamarchi, Phys. Rev. B **85**, 235108 (2012).

[54] J. C. Slater and G. F. Koster, Phys. Rev. **94**, 1498 (1954).

[55] N. Marzari, A. A. Mostofi, J. R. Yates, I. Souza, and D. Vanderbilt, Rev. Mod. Phys. **84**, 1419 (2012).

[56] N. Marzari, I. Souza, and D. Vanderbilt, Highlight of the Month, Psi-K Newsletter **57**, 129 (2003).

[57] U. Schollwöck, Ann. Phys. (NY) **326**, 96 (2011).

[58] T. Maier, M. Jarrell, T. Pruschke, and M. H. Hettler, Rev. Mod. Phys. **77**, 1027 (2005).

[59] A. Kokalj, Comput. Mater. Sci. **28**, 155 (2003).

[60] I. V. Solovyev, J. Phys.: Condens. Matter **20**, 293201 (2008).

[61] M. Imada and T. Miyake, J. Phys. Soc. Jpn. **79**, 112001 (2010).

[62] K. Held, I. A. Nekrasov, N. Blümer, V. I. Anisimov, and D. Vollhardt, Int. J. Mod. Phys. B **15**, 2611 (2001).

[63] C. Gros and R. Valenti, Phys. Rev. B **48**, 418 (1993).

[64] D. Sénéchal, D. Perez, and M. Pioro-Ladrière, Phys. Rev. Lett. **84**, 522 (2000).

[65] M. Aichhorn, H. G. Evertz, W. von der Linden, and M. Potthoff, Phys. Rev. B **70**, 235107 (2004).

[66] M. Aichhorn, E. Y. Sherman, and H. G. Evertz, Phys. Rev. B **72**, 155110 (2005).

[67] M. Potthoff, M. Aichhorn, and C. Dahnken, Phys. Rev. Lett. **91**, 206402 (2003).

[68] L. Chioncel, H. Allmaier, E. Arrigoni, A. Yamasaki, M. Daghofer, M. I. Katsnelson, and A. I. Lichtenstein, Phys. Rev. B **75**, 140406 (2007).

[69] M. Aichhorn, T. Saha-Dasgupta, R. Valentí, S. Glawion, M. Sing, and R. Claessen, Phys. Rev. B **80**, 115129 (2009).

[70] V. I. Anisimov, A. I. Poteryaev, M. A. Korotin, A. O. Anokhin, and G. Kotliar, J. Phys.: Condens. Matter **9**, 7359 (1997).

[71] M. I. Katsnelson and A. I. Lichtenstein, J. Phys.: Condens. Matter **11**, 1037 (1999).

[72] L. Chioncel, M. I. Katsnelson, R. A. de Groot, and A. I. Lichtenstein, Phys. Rev. B **68**, 144425 (2003).

[73] J. C. Slater, Phys. Rev. **51**, 846 (1937).

[74] O. K. Andersen, Phys. Rev. B **12**, 3060 (1975).

[75] D. Singh, Phys. Rev. B **43**, 6388 (1991).

[76] E. Sjöstedt, L. Nordström, and D. Singh, Solid State Commun. **114**, 15 (2000).

[77] P. Hohenberg and W. Kohn, Phys. Rev. **136**, B864 (1964).

[78] W. Kohn and L. J. Sham, Phys. Rev. **140**, A1133 (1965).

[79] P. Blaha, K. Schwarz, G. Madsen, D. Kvasnicka, and J. Luitz, WIEN2K, An Augmented Plane Wave + Local Orbitals Program for Calculating Crystal Properties (Karlheinz Schwarz, Techn. Universität Wien, Austria, Wien, Austria, 2001).

[80] For a simplification of the calculation, in particular the structure of the k mesh, we approximated β to 90.0°. We checked that the band structure is indistinguishable along the high-symmetry directions.

[81] D. M. Ceperley and B. J. Alder, Phys. Rev. Lett. **45**, 566 (1980).

[82] J. P. Perdew, K. Burke, and Y. Wang, Phys. Rev. B **54**, 16533 (1996).

[83] N. W. Ashcroft and N. D. Mermin, *Solid State Physics* (Saunders College, Philadelphia, 1976).

[84] J. W. Allen (private communication).

[85] A. A. Mostofi, J. R. Yates, Y.-S. Lee, I. Souza, D. Vanderbilt, and N. Marzari, Comput. Phys. Commun. **178**, 685 (2008).

[86] J. Kunes, R. Arita, P. Wissgott, A. Toschi, H. Ikeda, and K. Held, Comput. Phys. Commun. **181**, 1888 (2010).

[87] E. Pavarini, I. Dasgupta, T. Saha-Dasgupta, O. Jepsen, and O. K. Andersen, Phys. Rev. Lett. **87**, 047003 (2001).

[88] All densities are given in terms of orbital densities $\langle n_i \rangle = \sum_\sigma \langle n_{i\sigma} \rangle$.

[89] Setting the maximum hopping range to fourth-nearest-neighbor unit cells in b, second-nearest-neighbor in c, and nearest neighbor in the a direction, we obtained 2160 single-particle matrix elements $M_{\mathbf{R}\alpha\mathbf{R}'\beta}$. We do not provide a full table of all matrix elements in this text. They are available upon request from aichhorn@tugraz.at.

[90] Since we start from a spin-symmetric calculation, $H_{\text{Wannier},\alpha\beta}$ is independent of spin σ.

[91] When numerically evaluating $\hat{\tilde{\mathcal{H}}}_{\text{AA}}(\mathbf{k})$, we use $(\omega - \hat{\mathcal{H}}_{\text{BB}})^{-1} \approx (\epsilon_{\text{AA}} - \hat{\mathcal{H}}_{\text{BB}} + i0.05)^{-1}$ followed by a Hermitization of the effective Hamiltonian $\tilde{\mathcal{H}}_{\text{AA}} = \frac{\tilde{\mathcal{H}}_{\text{AA}} + \tilde{\mathcal{H}}_{\text{AA}}^T}{2}$ for stability.

[92] D. A. Ryndyk, A. Donarini, M. Grifoni, and K. Richter, Phys. Rev. B **88**, 085404 (2013).

[93] C. Dahnken, M. Aichhorn, W. Hanke, E. Arrigoni, and M. Potthoff, Phys. Rev. B **70**, 245110 (2004).

[94] D. Senechal, arXiv:0806.2690.

[95] M. Aichhorn, E. Arrigoni, M. Potthoff, and W. Hanke, Phys. Rev. B **74**, 235117 (2006).

[96] A. Georges, G. Kotliar, W. Krauth, and M. J. Rozenberg, Rev. Mod. Phys. **68**, 13 (1996).

[97] M. Ferrero and O. Parcollet, TRIQS: a Toolbox for Research in Interacting Quantum Systems, http://ipht.cea.fr/triqs

[98] P. Werner, A. Comanac, L. de' Medici, M. Troyer, and A. J. Millis, Phys. Rev. Lett. **97**, 076405 (2006).

[99] P. Werner and A. J. Millis, Phys. Rev. B **74**, 155107 (2006).

[100] L. Boehnke, H. Hafermann, M. Ferrero, F. Lechermann, and O. Parcollet, Phys. Rev. B **84**, 075145 (2011).

[101] E. Gull, A. J. Millis, A. I. Lichtenstein, A. N. Rubtsov, M. Troyer, and P. Werner, Rev. Mod. Phys. **83**, 349 (2011).

[102] K. S. D. Beach, arXiv:cond-mat/0403055.

[103] T. Miyake, F. Aryasetiawan, and M. Imada, Phys. Rev. B **80**, 155134 (2009).

[104] J. Ferber, K. Foyevtsova, H. O. Jeschke, and V. Roser, arXiv:1209.4466.

[105] When comparing results of different techniques (LDA, VCA, DMFT, ARPES), we first apply a rigid band shift of 0.03 eV to the LDA data to account for the $\langle n \rangle \approx 1.44$ filling (which matches the as-is ARPES results). In order to be consistent with these LDA data, the VCA and DMFT data have to be shifted further by an offset which is determined by the way k sums are handled in the respective methods. The chemical potential offset of the respective methods, determined for $U = 0$ eV, is ≈0.1 eV for VCA and ≈0.13 eV for DMFT.

[106] F. H. L. Essler, H. Frahm, F. Göhmann, A. Klümper, and V. E. Korepin, *The One-Dimensional Hubbard Model* (Cambridge University Press, Cambridge, 2010).

[107] E. Hartmann, *An Introduction to Crystal Physics* (University College Cardiff Press, Cardiff, UK, 1984).

[108] V. S. Oudovenko, G. Pálsson, K. Haule, G. Kotliar, and S. Y. Savrasov, Phys. Rev. B **73**, 035120 (2006).

[109] J. M. Tomczak and S. Biermann, Phys. Rev. B **80**, 085117 (2009).

[110] X. Deng and J. Mravlje (private communication).

[111] Note that this may be a minimum, a maximum, or in general any stationary point in each of the parameters.

[112] Note that for largely delocalized orbitals, it is expected that the onsite interaction should be slightly larger in a more involved model that includes also off-diagonal Coulomb terms [113].

[113] M. Schüler, M. Rösner, T. O. Wehling, A. I. Lichtenstein, and M. I. Katsnelson, Phys. Rev. Lett. **111**, 036601 (2013).